

Experimental investigation of advanced multistage casing treatments in a 2.5 stage high pressure compressor test rig

T. Kroeckel, P. Jeschke
Institute of Jet Propulsion and Turbomachinery
RWTH Aachen University
D-52062 Aachen, Germany

S.J. Hiller
MTU Aero Engines GmbH
D-80995 Munich, Germany

Abstract

A two stage casing treatment was applied to a 2.5-stage axial compressor test rig and experimentally evaluated in terms of operability and local aerodynamics. The present study shows the impact of advanced casing treatments applied to both rotors of a compressor test rig, whose geometric and aerodynamic features are identical to those seen in the rear stages of an aircraft engine high pressure compressor. The casing treatment's impact on the local flow-phenomena, as well as their influence on the re-matching of the stage characteristics, is explained based on the experimental results presented. Furthermore, the performance of the compressor is analyzed.

The data presented shows how multiple casing treatments are generally able to extend the surge margin and furthermore operate under the influence of rotating stall. The impact of each casing treatment on the local flow and the operation of the test compressor is explained.

The present effort was conducted as part of the EU integrated program for New Aero Engine Core Concepts (NEWAC).

Nomenclature

I,0	Plane upstream of IGW	[-]
I,1	Plane upstream of R 1	[-]
I,2	Plane downstream of R 1	[-]
II,1	Plane upstream of R 2	[-]
II,2	Plane downstream of R 2	[-]
II,3	Plane downstream of S 2	[-]
SW	Smooth wall	[-]
CT	Casing treatment	[-]
A/D	Analog/Digital	[-]
IGV	Inlet Guide Vane	[-]
Ma	Mach number	[Ma]
P	Power input	[kW]
\dot{Q}_V	Heatflow	[kW]
R1,2	Rotor 1,2	[-]
R	Gas constant	[J/kgK]
RS	Rotating stall	[-]
EO	Engine order	[-]
S1,2	Stator 1, 2	[-]
OP	Operating point	[-]
TLV	Tip leakage vortex	[-]
T	Temperature	[K]
d	Diameter	[mm]
f	Frequency	[Hz]
h	Blade height	[mm]
\dot{m}	Mass flow rate	[kg/s]
n	Nominal rotational speed	[rpm]
p	Static pressure	[Pa]
u	Circumferential velocity	[m/s]
w	Relative velocity	[m/s]
c	Absolute velocity	[m/s]

Greek symbols

Π	Pressure ratio	[-]
Δ	Delta	[-]
δ	Tip clearance	[mm]
η	Efficiency	[-]
σ	Solidity	[-]
κ	Ratio of specific heat	[-]

Subscripts

h	Hub
is	Isentropic
ref	Reference
t	Total, dimensionless time, tip
s	Static
TM	Torque meter
bear	Bearing
I	Inlet

Introduction

An instrument to address the demand for safe and stable compressor operation is a casing treatment, which is well known to have the ability to increase the surge margin¹. In the past, most casing treatment designs were rather simple, consisting of geometries such as axial or skewed slots^{2,3} and single or multiple circumferential grooves^{2,4}. While these designs were able to extend the operational range of the tested compressors, they had a common tendency to reduce compressor efficiency. Recirculating casing treatments, which are more complex, have found to have the potential to reduce performance losses^{5,6}. Although most studies were performed with single stage casing treatments, some attempts to investigate multistage behavior were carried out by applying multiple stage recirculations⁷.

A self-recirculating casing treatment⁸ (see Figure 1) was applied to both stages of a 2.5 stage compressor test rig. The casing treatment used is an adaptation of a casing treatment described in Reference 6. While a previous publication⁹ covered aspects of the multi-CT setup over regular operation ranges, this paper explains how CTs interact in a compressor at close stall conditions. Flow phenomena that lead to a changed compressor map as well as the mechanism which leads to compressor stall are explained.

Experimental Setup

The results presented were obtained from a 2.5 stage axial compressor test rig which is designed to represent the final stages of a modern jet engine high pressure compressor¹⁰. Two integrally bladed rotors are installed with 24 (R1) and 32 (R2) blades. Each stator has 40 vanes with a fixed stagger angle and is designed with tip and hub shrouds. An overview of the actual rig setup is given in Figure 2. A pressure controller is used to provide a constant total pressure at the compressor inlet for different mass flow rates.

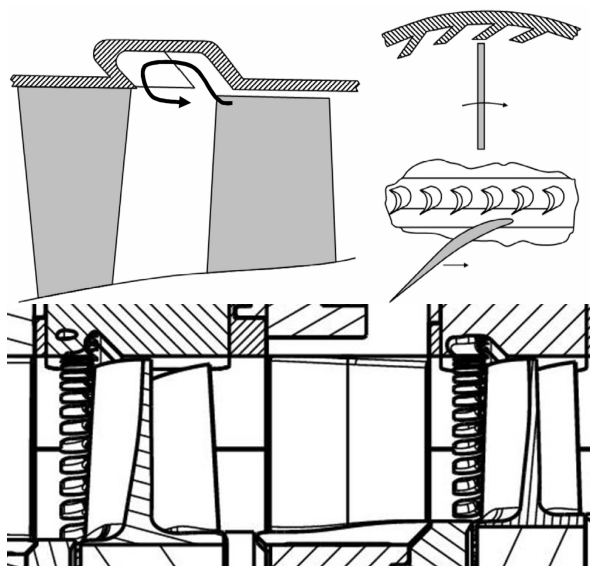


Figure 1. Conceptual drawing of the casing treatment^{6,8} and the casing treatment installed at the test rig¹¹

Multiple measurement techniques were applied to the test rig to examine the influence of the casing treatment on the compressor's performance^{8,9}. Furthermore, a calibrated Venturi nozzle was used to determine the mass flow rate. By considering the torque of the rotor and the losses in the journal bearings it was possible to calculate the efficiency of the compressor.

$$\eta_{t,is,mech} = \frac{\kappa}{\kappa-1} \dot{m} R T_{t,1} \left[\Pi^{\left(\frac{\kappa-1}{\kappa}\right)} - 1 \right] / (P_{TM} - \dot{Q}_{V,bear})$$

At conditions shown in the table below, the efficiency was determined with a relative uncertainty of 0.35%.

Nominal rotational speed	n	14958	rpm
Total pressure ratio	Π_t	1.67	-
Absolute mass flow	\dot{m}	7.70	kg/s
Isentropic efficiency	$\eta_{t,is}$	89.50	%
Power input	P	422	kW
Total temperature rise	ΔT_t	52.7	K
Inner casing diameter	d	385.43	mm
Rotor tip speed	u	302.40	m/s
Tip clearance R1	δ_{R1}	0.70	mm
Tip clearance R2	δ_{R2}	0.75	mm
Average stage reaction	ρ_h	0.69	-
Average aspect ratio (w/o IGV)	AS	0.95	-
Average hub/tip ratio	d_h/d_t	0.75	-
Reynolds number R1	Re_{R1}	9.0 E5	-
Average rel. rotor inlet Ma number (tip)	Ma_w	0.86	-
Average abs. stator inlet Ma number (hub)	Ma	0.56	-
Tip clearance relative to blade height R1	δ/h	1.4	%
Tip clearance relative to blade height R2	δ/h	1.6	%
Number of blades R1		24	-
Number of blades R2		32	-
Number of blades IGV, S1, S2		40	-
5-Hole Probe diameter	d_{shp}	2.5	mm

Table 1: Compressor specifications

The measurements were conducted on a rig configuration with smooth walls and another one with installed casing treatments. The present study focuses on effects that appear at high rotor speeds. Therefore, the majority of the measurements were carried out at aerodynamic speeds from 83% to 97% of the design speed. Measurements at the 100% speed line were ruled out due to excitations of the IGV. Besides the performance measurements, results obtained from three additional techniques will be discussed in this paper.

Static pressure measurements

Multiple static pressure taps were applied to the outer wall of each

casing treatment (see Figure 5). The pressure data was recorded at multiple points along with the speed lines at 83%, 90%, 95% and 97% rotor speed.

Flow traverses

Furthermore, extensive five-hole probe measurements were performed at all four speed lines using automated traversing units. As many as 24 operating points for both rig configurations were examined. In contrast to the results presented in Reference 9, the resolution of the measurement grid was reduced due to the increased amount of operating points. At measurement planes (see Figure 2) downstream of a stator, the grid consisted of 10 radial and 6 circumferential points with an extent of 7.5°. At every other measurement plane a single radial traverse of 10 points was performed. In order to get comparable results for both configurations, the mass flow rate was kept constant for each operating point. Since the condition close to the surge line is of highest interest, only operating points shown in Figure 4 are discussed in this paper.

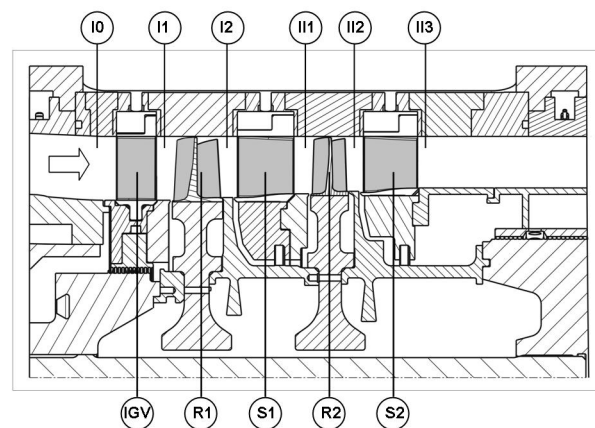


Figure 2. 2.5 stage compressor test rig

Unsteady pressure measurements

In addition, at 50% axial chord of each rotor, high-frequency response pressure transducers (Kulite XCE-62-25) were mounted flush to the casing (see Figure 3). A multiplexer with a cut-off frequency of 109,650 Hz was used to amplify the Kulite signal. The signal was recorded by a PC with a built-in A/D converter card at a sample rate of 200 kHz.

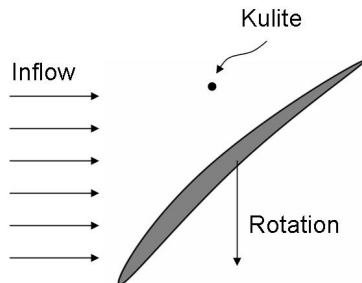


Figure 3. Relative position of the pressure transducer

Compressor Map

The influence of the CT on the performance of the compressor can be best seen by comparing the speed lines of both configurations in the compressor map (see Figure 4). The surge margin is significantly extended relative to the configuration with smooth casing walls. While the CT speed lines show a minor offset at de-throttled operating ranges, as throttling is increased, the compressor tends to deliver a higher pressure ratio at the same mass flow rate. The efficiency on the other side remains mostly unaffected by the influence of the CT.

All speed lines measured at the baseline configuration indicate compressor stall at the highest pressure ratio. A similar behavior, although at a higher pressure level, can be seen at the 83% and 90% speed lines for the compressor equipped with casing treatments. At

95% and 97% speed, the surge margin is even further increased. Instead, the compressor runs at secondary and tertiary characteristics as described in Reference 12. Both speed lines get to a point with a horizontal pressure gradient, where rotating stall was generated which partially blocked the compressor cross-section.

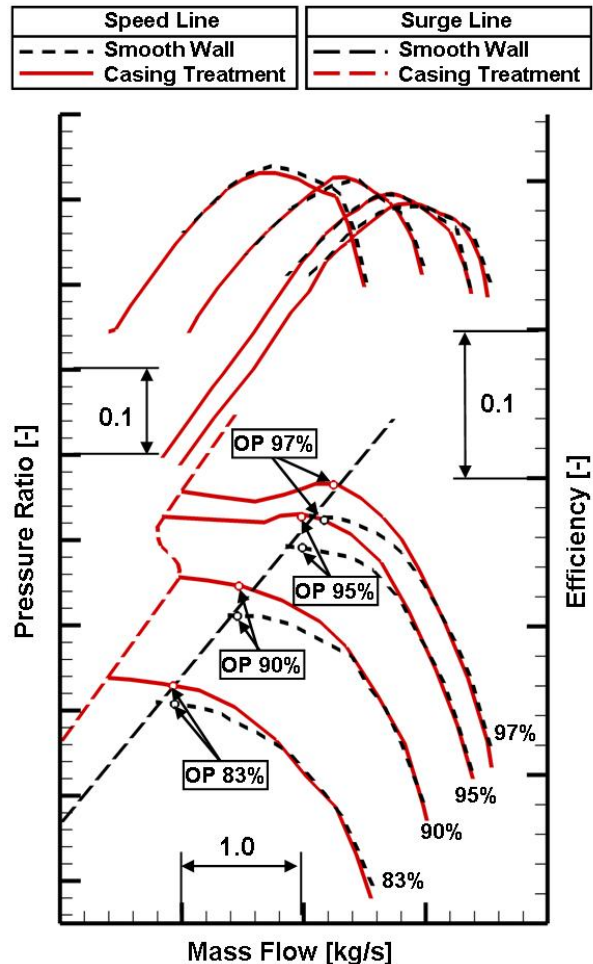


Figure 4. Compressor map

Further throttling led to a lower total pressure ratio, where the compressor operated on secondary characteristics. Once the pressure began to rise again, a full ring stall was established and the compressor operated on the tertiary characteristics until full surge occurred. The origin of this effect will be explained in the following section.

Wall pressure at the CT

Since the indirect influence of the CT to the main flow field can be very well described with the help of 5-hole-probe measurements⁹, signs of the direct influence have to be found in the CT itself. Therefore, 6 static pressure taps have been applied to the outer wall of each casing treatment (Figure 5).

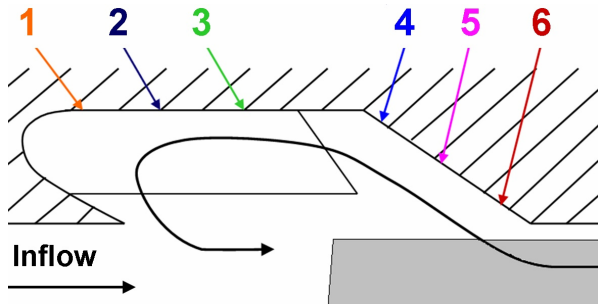


Figure 6. Position of pressure taps on the wall of a casing treatment

As seen in Figure 6, the wall pressure of each CT is plotted as a bundle of 6 pressure lines over the compressor mass flow rate for four rotor speeds. The color notation for each pressure line can be seen in Figure 5. For better comparison, the speed lines of the CT and the SW configuration were added to the figure. While throttling the compressor towards the surge line, the pressure measurements were triggered manually starting at low mass flow rates and ending randomly at a point close to the surge line. As a common characteristic, a relatively dense distribution of all pressure lines of each CT can be seen at high mass flow rates. Until this point, the wall pressure at the CT is roughly at the same level of static pressure of the main rotor flow. Advancing towards higher pressure ratios and lower mass flow rates all CT pressure lines start to diverge. This occurs exactly where the speed lines of the CT configuration and the SW configuration start to separate and

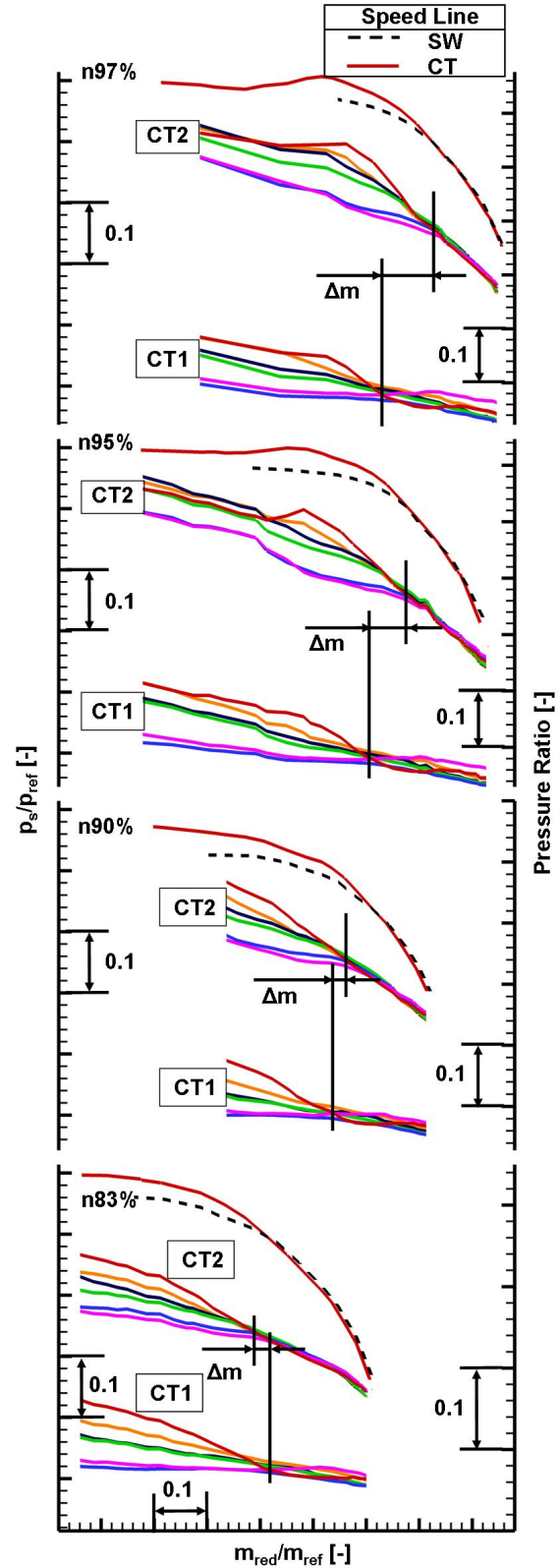


Figure 5. Static wall pressure distribution at both CTs in comparison with speed lines

marks the point where the CTs start to have an impact on the compressor flow. The radically changing pressure distribution can be explained by a changed flow velocity within the CT.

Measurements shown in Reference 9 indicated a reduced intensity of the tip leakage vortex downstream of both rotors by the influence of the CT. Since the driving force for the TLV is the pressure difference between the suction and pressure side of the rotor blade, it can be assumed that with an increased blade loading the trajectory of the TLV moves towards the leading edge and an increasingly larger fraction of the TLV is shifted into the cavity of the CT, which leads to higher velocities within the CT and therefore the rising differences of the pressure lines. While the pressure lines at 83% and 90% rotor speed indicate a constantly increasing strength of the TLV in the CT, the lines at 95% and 97% show a different behavior.

As mentioned previously, the characteristic of the 95% and 97% speed lines is an indication for partial blocking of the compressor cross-section at some point. With the information obtained from the CT-wall pressure, a formation of a ring stall at the tip of the second rotor can be assumed. In the region of the point of peak pressure ratio, a reduced spreading of the rotor two CT-pressure lines indicate a reduction in the effectiveness of the CT caused by local flow separation in the vicinity of the CT. Beyond this point the spreading of the pressure lines remains constant, therefore, the recirculation in the CT has to be maintained to some extent. The partial blocking at the second rotor has a throttling effect to the upstream stages.

Although the secondary and tertiary characteristics can be described by the effects of the ring stall, the

change between the 90% and 95% speed lines has a different origin. Since the effectiveness of the applied CT depends on the aerodynamic loading of the rotor blade involved, the spreading of the CT-pressure lines is a good measure of the actual blade load. In Figure 6, at each bundle of CT-pressure lines a characteristic point is marked. Comparing these points at CT 1 and CT 2 for different rotor speeds it becomes obvious that as the rotor speed rises the loading is increased in rotor two relative to rotor one (indicated by the Δ). While at higher rpm and with the first sign of rotating stall at rotor two, the first rotor is far from its critical operation. Rotor one is able to compensate for the throttling effect of the ring stall at rotor two and stabilizes the whole compressor.

Probe Traverses

While the pressure measurements taken at the wall of the CT gave a good impression of the local flow phenomena, the changes of the whole flow field need to be verified with a more extensive measurement technique. Therefore, five-hole probes were traversed at every measurement plane. For the present work, only the results obtained at operating points close to the surge line were evaluated (see Figure 4). The mass flow rate for each operating point was kept constant at both configurations. Although the operating points compared were set to be equally close to the surge line, they do not necessarily represent equal flow conditions. Therefore, comparability is limited but good enough to explain certain flow phenomena.

Since the CT was found to have the greatest impact on the rotor flow field⁹, the diffusion factor as a characteristic parameter of blade loading will be discussed in this

section. The diffusion factor is defined as follows:

$$DF = 1 - \frac{w_2}{w_1} + \frac{w_{u1} - w_{u2}}{2\sigma w_1}$$

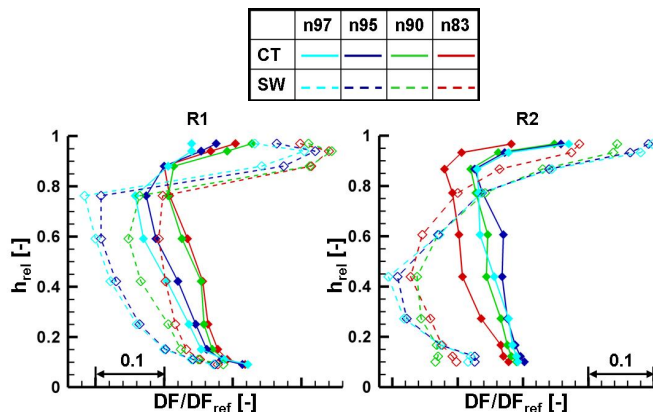


Figure 7. Normalized Diffusion Factor of rotor one and two at four rotor speeds and at an operating point close to the surge line

The distribution of the diffusion factor of both rotors is shown in Figure 7. At first, the direct impact of the CT to the main flow field is limited to the reach of the TLV - in this case the upper 20% of the blade height. Furthermore, it can commonly be seen that above 80% the DF is reduced due to the influence of the CT, while below 80% the DF is increased. The compressor equipped with CTs is known to deliver a higher pressure ratio at these operating points (see Figure 4) and therefore the integral loading of the rotor blades has to be higher than without the CTs. This effect can be seen very well at both rotors. On the other side, the influence of the different rotor speed leads to a difference between the rotors. Similar to the findings in the previous section, the DF distribution of the first rotor verifies a reduced blade loading for higher rotor speeds. In contrary the loading of the second rotor remains relatively unaffected by the changes of the rotor speed.

Unsteady wall pressure

In order to determine the pressure fluctuations which appear at close-stall conditions and gain further understanding of the interaction of the stages, high frequency pressure transducers were mounted on the casing of both rotors. The signals of the sensors were sampled at 200 kHz and simultaneously recorded on a PC. Three techniques were used to analyze the pressure signals. At first, large scale fluctuations were analyzed with the help of the raw unsteady pressure signal. Furthermore a frequency distribution is shown. Finally, the influence of single stall cells is studied. Therefore, a filtering method was applied to the unsteady pressure signal in order to eliminate the impact of single blade passes.

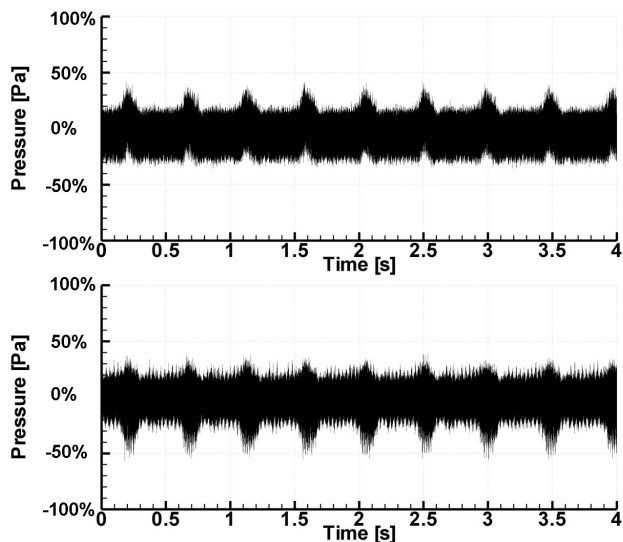


Figure 8. Unsteady wall pressure readings from rotor one (top) and rotor two (bottom) at 97% speed (CT configuration)

As described in the previous section, due to the rotating stall the CT at the second rotor will eventually lose some of its effectiveness. In Figure 8 the pressure signals from both rotors

recorded at 97% rotor speed are shown at the moment when RS starts to appear. At this point the formation of the stall is not stable, it is rather a sequence of short bursts lasting only about 0.2 seconds (equivalent to about 50 rotor revolutions). During this time the signal of the second rotor is clearly expanded while the pressure at the first rotor is slightly raised. This observation confirms the finding of the previous section: part span stall and throttling effect at the second rotor while the first rotor is able to compensate this with a higher loading.

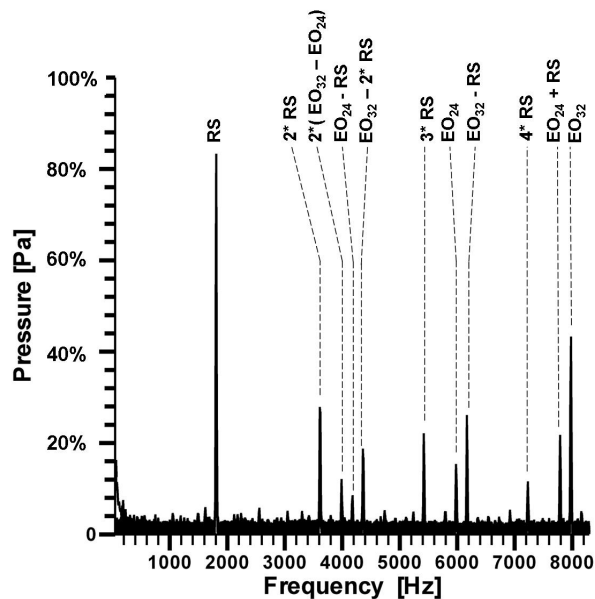


Figure 9. Frequency analyses of the wall pressure signal at 97% rotor speed at conditions close to the surge line (CT configuration)

Although the stall was not stable at the beginning, if the throttle was further closed, the stalling periods lasted longer and finally the compressor operated with a stable part span stall at rotor two. In Figure 9, the frequency distribution of a pressure signal which was recorded just before surge at 97% rotor speed is shown

at the CT configuration. Besides the blade passing frequency (R1 6100Hz, R2 8000Hz) a significant peak at about 1800Hz can be seen. Since this frequency only appears while the compressor operates close to the surge point, this can be determined as the frequency of the rotating stall. The very narrow line at the RS-frequency is an indication of a very stable rotating stall configuration with a fixed number of stall cells and constant rotational speed. Although not shown in Figure 9, the rotating stall frequency is also the dominating frequency at the pressure signal of rotor one. Measurements at the SW-configuration showed RS to be the stall inception mechanism for 95% and 97% rotor speed, leading almost immediately to full surge. This can be seen as an indication that even without casing treatments the first rotor was to some extent able to compensate RS at rotor two. Two CTs applied to the compressor were not able to prevent rotating stall, but prevented rotating stall from pushing the compressor to full surge right away.

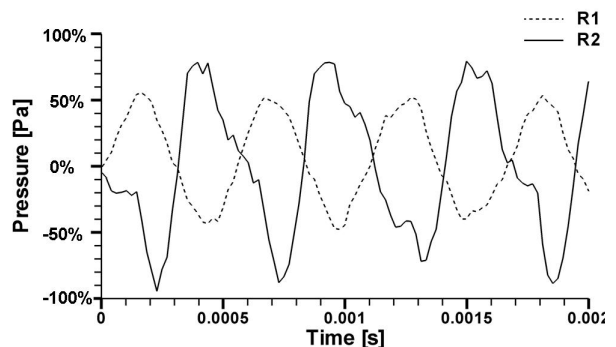


Figure 10. Comparison of unsteady wall pressure readings from rotor one and rotor two at 97% rotor speed at conditions close to the surge line (CT configuration)

The rotating stall itself causes pressure fluctuations at a fairly small scale. In order to analyze these effects, the pressure signal which was recorded at both rotors and at the same circumferential

position is compared in Figure 10. Since only the pressure fluctuations caused by the stall are of interest, the signals were scaled to the same level and filtered to eliminate the influence of single blade passings.

Comparing both signals, two main differences become apparent. The pressure signal at rotor two has a higher amplitude and is less uniform than the signal of rotor one. The alternating pressure at rotor two is caused by moving stall cells. Each time pressure values at rotor two are relatively low, a stall cell is right on top of the sensor causing a partial blocking of the rotor passage. As seen before on a larger scale, the first rotor responds with a pressure rise.

Conclusions

1. Multiple casing treatments are able to delay the full surge caused by rotating stall and therefore lead to a further extended surge margin.
2. The surge margin of a high tip loading multistage compressor can be effectively increased by the use of casing treatments applied to the casing of each rotor.
3. A well designed recirculating casing treatment does not have degrading effects on compressor efficiency at the aerodynamic design point.
4. The compressor configuration with casing treatments causes a significantly changed surge margin at 95% and 97% rotor speed.
5. The casing treatment that was used for the present study is able to stabilize the rotating part span stall.

Acknowledgements

The authors would like to thank MTU Aero Engines GmbH and the other NEWAC partners for their permission to publish this paper. The authors also wish to thank the EU for supporting this project - the work was funded under the EU contract number AIP5-CT-2006-030876.

References

- [1] Hathaway, M.D., 2007, "Passive endwall treatments for enhancing stability", NASA Report TM-2007-214409
- [2] Osborn, W.M, Lewis, G.W., Heidelberg, L.J., 1971, "Effect of several porous casing treatments on stall limit and overall performance of an axial compressor rotor", NASA Report TN 6537
- [3] Wilke, I., Kau H-P., 2004, "A numerical investigation of the flow mechanisms in a high-pressure compressor front stage with axial slots", ASME J. Turbomachinery
- [4] Houghton, T., Day, I., 2009, "Enhancing the stability of subsonic compressors using casing grooves", ASME paper GT2009-59210
- [5] Zscherp, C., 2008, "Aerodynamische Verdichterauslegung unter Berücksichtigung stabilitätsverbessernder Maßnahmen", Sierke Verlag, Goettingen, ISBN 978-3-86844-095-9
- [6] Engel, K., Zscherp, C., Wolfrum, N., Nürnberger, D., Kügeler, E., 2009, "CFD Simulations of the TP400 IPC with Enhanced Casing Treatment in Off-Design Operating Conditions", ASME paper GT2009-60324
- [7] Strazisar, A.J., Bright, M.M., Thorp, S., Culley,

- D.E., Suder, K.L., 2004,
"Compressor stall control
through endwall
recirculation", ASME paper
GT2004-54295
- [8] Seitz, P., 2005,
"Recirculation Structure for
Turbo Chargers", US Patent
6935833 B2, MTU Aero Engines
GmbH, Munich, Germany
- [9] Kroeckel, T., Hiller, S.J.,
Jeschke, P., 2011,
"Application of a Multistage
Casing Treatment in a High
Speed Axial Compressor Test
Rig", ASME Paper GT2011-46315
- [10] Ernst, M., Michel, A.,
Jeschke, P., 2009, "Analysis
of Rotor-Stator-Interaction
and Blade-to-Blade
Measurements in a Two Stage
Axial Flow Compressor", ASME
paper GT2009-59371
- [11] Kroeckel, T., 2010,
"Multistage Casing Treatment
at High Pressure Compressor
Rear Stages", Workshop
Presentation, European
Workshop on New Aero Engine
Concepts
- [12] Cumpsty, N.A., 2004,
"Compressor Aerodynamics",
Krieger Publishing Company